

GCIRS 7, a pulsating M1 supergiant at the Galactic Centre^{★,★★}

Physical properties and age

T. Paumard¹, O. Pfuhl², F. Martins³, P. Kervella¹, T. Ott², J.-U. Pott⁴, J.B. Le Bouquin⁵, J. Breittfelder^{1,6}, S. Gillessen², G. Perrin¹, L. Burtscher², X. Haubois¹, and W. Brandner⁴

¹ LESIA, Observatoire de Paris, CNRS, UPMC, Université Paris-Diderot, PSL research university, 5 place Jules Janssen, 92195 Meudon, France

e-mail: thibaut.paumard@obspm.fr

² Max-Planck-Institut für extraterrestrische Physik, D-85748 Garching, Germany

e-mail: pfuhl@mpe.mpg.de

³ LUPM, Université Montpellier 2, CNRS, Place Eugène Bataillon, F-34095, Montpellier, France

⁴ Max-Planck-Institut für Astronomie, Königstuhl 17, 69117 Heidelberg, Germany

⁵ Univ. Grenoble Alpes, IPAG, F-38000 Grenoble, France

CNRS, IPAG, F-38000 Grenoble, France

⁶ European Southern Observatory, Alonso de Córdova 3107, Casilla 19001, Santiago 19, Chile

TBD

ABSTRACT

Context. The stellar population in the central parsec of the Galaxy is dominated in mass and number by an old (several Gyr) population, but young (6 ± 2 Myr), massive stars dominate the luminosity function. The most luminous of these stars is a M1 supergiant, GCIRS 7.

Aims. We have studied GCIRS 7 in order to constrain the age of the recent star formation event in the Galactic Centre and to characterise it as a visibility and phase reference for observations of the Galactic Centre with the interferometric instrument GRAVITY, which will equip the Very Large Telescope Interferometer (VLTI) in the near future.

Methods. We present the first H-band interferometric observations of GCIRS 7, obtained using the PIONIER visitor instrument on the VLTI using the four 8.2-m unit telescopes. In addition, we present unpublished K-band VLTI/AMBER data and build JHKL light-curves based on archival data spanning almost 40 years, and measured the star's effective temperature using SINFONI integral field spectroscopy.

Results. GCIRS 7 is marginally resolved at H-band, with a uniform-disk diameter $\theta_{\text{UD}}(2013) = 1.076 \pm 0.093$ mas ($R_{\text{UD}}(2013) = 960 \pm 92 R_{\odot}$ at 8.33 ± 0.35 kpc). We detect a significant circumstellar contribution at K-band. The star and its environment are variable in brightness and in size. The photospheric H-band variations are well modelled with two periods: $P_0 \approx 470 \pm 10$ days (amplitude ≈ 0.64 mag) and long secondary period $P_{\text{LSP}} \approx 2700\text{--}2850$ days (amplitude ≈ 1.1 mag). As measured from ^{12}CO equivalent width, $\langle T_{\text{eff}} \rangle = 3600 \pm 195$ K.

Conclusions. The size, periods, luminosity ($\langle M_{\text{bol}} \rangle = -8.44 \pm 0.22$) and effective temperature are consistent with an M1 supergiant with an initial mass of $22.5 \pm 2.5 M_{\odot}$ and an age of 6.5–10 Myr (depending on rotation). This age is in remarkable agreement with most estimates for the recent star formation event in the central parsec. Caution should be taken when using this star as a phase reference or visibility calibrator as it is variable in size, is surrounded by a variable circumstellar environment and large convection cells may form on its photosphere.

Key words. galaxy: nucleus – supergiants – stars: individual: GCIRS 7 – techniques: interferometric – techniques: photometric – techniques: spectroscopic

1. Introduction

The central parsec of the Milky Way galaxy is host of a dense star cluster which is made of a relaxed population of late-type stars intermixed with a much younger population of luminous, evolved, massive stars (Genzel et al. 2010, and references

therein). About one hundred of those young stars seem to be born in one single event of star formation, presumably within a massive self-gravitating accretion disk which is hypothesised to have existed at that time around the super-massive black-hole candidate Sgr A* (Paumard et al. 2006; Bartko et al. 2009; Lu et al. 2013, and references therein).

[★] This work relies on interferometric, spectroscopic and imaging data obtained at the VLT and VLTI in Cerro Paranal Chile between 2003 and 2013. The observations were carried out under the program-ids 075.B-0547, 076.B-0259, 077.B-0503, 179.B-0261, 381.D-0529, 183.B-0100, 087.B-0117, 087.B-0280, 088.B-0308, 288.B-5040, and 091.D-0682.

^{★★} This work was supported by the French ANR POLCA project (Processing of pOLychromatic interferometriC data for Astrophysics, ANR-10-BLAN-0511).

GCIRS 7 is by far the brightest star in the Galactic Centre (GC) at H and K band. This M1 supergiant (Blum et al. 1996b) has been first observed in 1966 by Becklin & Neugebauer (1968, 1975). Interstellar medium (ISM) features North of the source are interpreted as the outer layers of the star's atmosphere being blown away by the central cluster wind in a cometary tail (Serabyn et al. 1991; Yusef-Zadeh & Morris 1991). This star

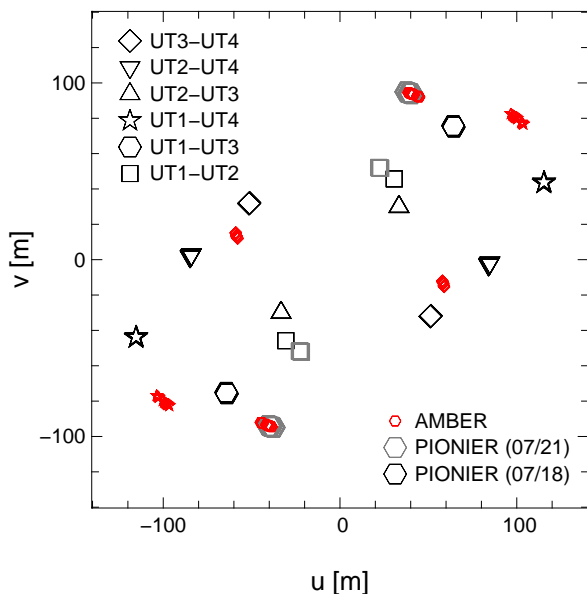


Fig. 1. Projected baselines ((u, v) coverage) of the PIONIER (*large symbols*) and AMBER (*small symbols*) data.

is in itself an interesting target: it is the brightest of the very few current-day red supergiant (RSG) stars presumably formed together with the disk of young stars in the GC (Krabbe et al. 1995). It also interacts with a wind from either the hot stars or perhaps the black-hole vicinity itself.

In addition, GCIRS 7 is an important star for future observations in the GC. It has often been used as wave-front reference for infrared adaptive optics systems such as NAOS, and will be used again for that purpose for interferometric observations with the 4-telescope beam combiner GRAVITY (Eisenhauer et al. 2008). It will also very likely be used as a fringe-tracker and phase reference for certain GC observations involving the 1.8-m auxiliary telescopes (ATs). It is therefore timely to study its interferometric structure and behaviour.

Pott et al. (2008) have observed the star using AMBER at K-band and MIDI at N-band. They find that the star is marginally resolved at K-band, more so than its photospheric luminosity would suggest, and strongly resolved at N-band. They conclude that dust surrounding the star dominates the visibility in the mid-infrared and has a non-negligible contribution in the near-infrared.

Blum et al. (1996a) have shown that the luminosity of GCIRS 7 has increased by approximately 0.8, 0.5 and 0.3 magnitudes at J, H and K-band respectively between 1978 and 1993. Ott et al. (1999) have measured a K-band luminosity decrease of 0.7 magnitudes between 1992 and 1998. Those authors have not been able to determine any particular regularity in the light-curve and have classified GCIRS 7 as a long-period variable (LPV) supergiant.

In Sect. 2, we describe our original and archival data sets. In Sect. 2.3, we derive stellar parameters such as the size and effective temperature, interferometric and photometric variations, age and mass of the star (Table 1). We discuss our findings in Sect. 4.

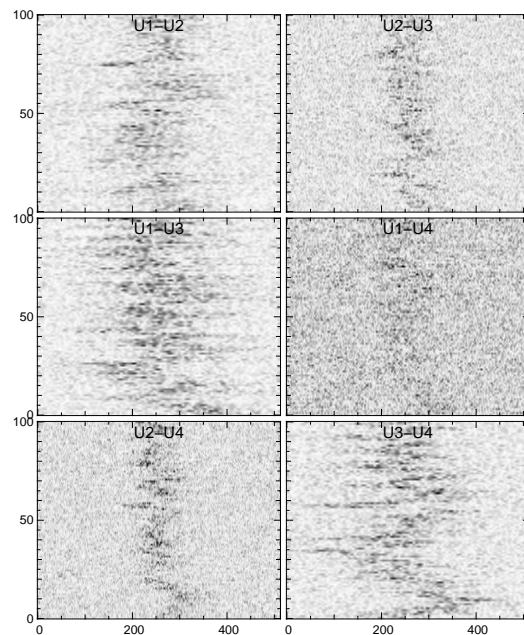


Fig. 2. Example fringe waterfalls for one exposure. Each panel corresponds to one telescope pair. In each panel, the vertical axis corresponds to scan number (one scan lasts ≈ 1 s) and the horizontal axis to index within scan (which corresponds to optical path difference). In this specific example, fringes are present on all baselines.

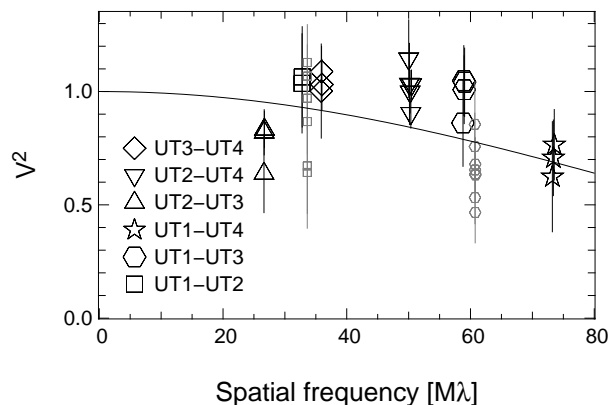


Fig. 3. 2013 H-band PIONIER data, V^2 vs. spatial frequency in $10^6/\text{rad}$ or $M\lambda$. *Solid line*: uniform-disk model of diameter 1.076 mas. *Larger, black symbols*: first night, *smaller, grey symbols*: second night.

2. Observations

2.1. Interferometry

2.1.1. PIONIER 2013

We have observed the star using PIONIER (Le Bouquin et al. 2011) using the four 8.2-m Unit Telescopes (UTs) of the VLTI on July 18th and 21st, 2013. We used an optical wave-front reference star about $15''$ north-East of the target (USNO-A2.0 0600-28577051). The (u, v) coverage is shown on Fig. 1. Since we wanted to observe fairly faint targets with off-axis adaptive optics, we used the H-band undispersed mode of the instrument.

The atmospheric conditions on the first night were partly cloudy with fast coherence time (≈ 3 ms). We were nevertheless able to record fringes on all 6 baselines (Fig. 2) and to observe a good set of calibration stars. The second night was clearer, but coherence time was even shorter (≈ 1 ms) so that it proved impossible to stabilise the fringes, that we were able to witness

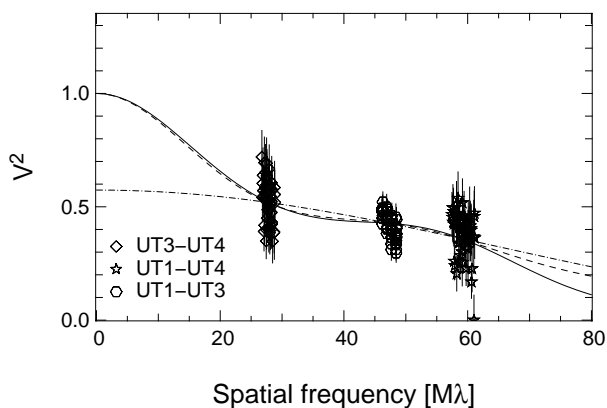


Fig. 4. 2008 K-band AMBER data, V^2 vs. spatial frequency in $10^6/\text{rad}$ or $M\lambda$. *Lines*: several two-components models where the star is represented by a uniform disk and the environment by one of: *solid line*: a circle, figuring a thin shell; *dashed line*: a second uniform disk, figuring a thick shell; *dash-dotted line*: a uniform background.

by eye, on the detector. We therefore searched for fringes on a brighter calibrator and then trusted the VLTI delay line model to apply the right offsets when pointing GCIRS 7. We then recorded scans blindly on the source. Indeed, several scans proved usable at data reduction time and confirm the visibilities measured on the first night.

The data have been reduced using the version 2.55 of the PIONIER pipeline `pndrs` (Le Bouquin et al. 2011). Since our target is at rather low signal to noise and in order to not introduce biases, we have decided to select scans where fringe detection is certain from a visual inspection of the scan waterfalls, but to not filter more within those scans as additional filtering may lead to biases.

In total, we have been able to obtain data for all six baselines on the first night and only for U1–U2 and U1–U3 (not at the same time) on the second night (Fig. 3). Closure phases were also measured on all three triplets on the first night, all compatible with 0° to within the uncertainties, as expected for an unresolved or marginally resolved source.

2.1.2. AMBER 2008

GCIRS 7 and the calibrator were observed with AMBER in low-resolution mode and frame exposure time (DIT) of 50 ms, on the night of May 17, 2008 with the VLTI-UT sub-array UT134. Fringes were recorded on all three baselines in service mode operation. The (u, v) coverage is shown on Fig. 1. Seeing was typically better than $1''$. Due to the high visual extinction towards the GC, off-axis adaptive optics guiding with MACAO was achieved with the nearby USNO-A2.0 0600-28577051. The visibility calibrator HD 164866 was observed close to the target (dist = 4.6°). HD 164866 is with $m_K = 6.5$ mag also of comparable K-band brightness to GCIRS 7.

The data reduction was performed following standard procedures described in Tatulli et al. (2007) and Chelli et al. (2009), using the `amdlib` package, release 3.0.8, and the `yorick` interface provided by the Jean-Marie Mariotti Center (JMMC)¹. First, raw spectral visibilities and closure phases were extracted for all the frames of each observing file. Then a selection of frames with piston smaller than $15 \mu\text{m}$ was made to achieve higher signal-to-noise ratio (SNR) on the visibilities and phases.

¹ The calibrated data in the OI-FITS format (Pauls et al. 2005) will be included in the JMMC database <http://www.jmmc.fr>.

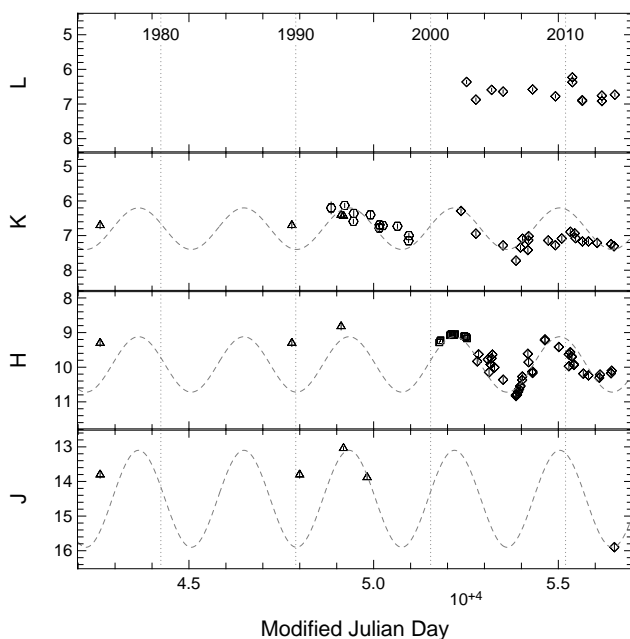


Fig. 5. J, H, Ks and L-band light-curves. The oldest data is from 1975, the latest from June 2013. Statistical uncertainties are represented, although they are often smaller than the symbol. *Diamonds*: NACO data; *squares*: from Peebles et al. (2007); *circles*: from Ott et al. (1999, these points have been brought up by 0.3 mag); *triangles*: from Blum et al. (1996a) which includes data from Becklin & Neugebauer (1975) and Depoy & Sharp (1991). *Dashed curves*: sinusoidal models with a period of 2850 d.

Note that GCIRS 7 was at the very limit of sensitivity of AMBER in 2008. Therefore we confirmed to get stable, calibrated results with two SNR-based frame selections (20%, Fig. 4, and 80%). The two frame selections within the piston-limited subset yield the same results, within the stated uncertainties, which is reassuring. The transfer function was obtained by averaging the calibrator measurements, after correcting for their intrinsic diameters. Here again, closure phases are statistically compatible with 0° .

2.2. Photometry

2.2.1. NACO Imaging Photometry

The photometric data were obtained with the adaptive optics camera NACO (Rousset et al. 2003; Lenzen et al. 2003). The images were taken between 2002 and 2013. Most of the images were taken with the H and Ks-band filters with the 13 mas/pixel or the 27 mas/pixel camera. Additional L-band and one J-band images were obtained with the 27 mas/pixel camera. Especially the H and Ks-band images were selected depending on the saturation level of GCIRS 7 in the image. Images with very good seeing and long integration times had to be removed because they were strongly affected by saturation. Each selected image was sky-subtracted as well as bad-pixel and flat-field corrected. In total we used 20 Ks-band, 39 H-band, 21 L-band and one J-band image with temporal spacing between one day and up to 11 years to construct the light-curve of GCIRS 7.

The photometry on the individual images was done by 2D Gaussian fits to the stars. As photometric references, the bright early-type stars GCIRS 16NE and GCIRS 16C were used. Both stars showed little or no variability over the recorded time base. We used the magnitudes stated by Blum et al. (1996a) as ref-

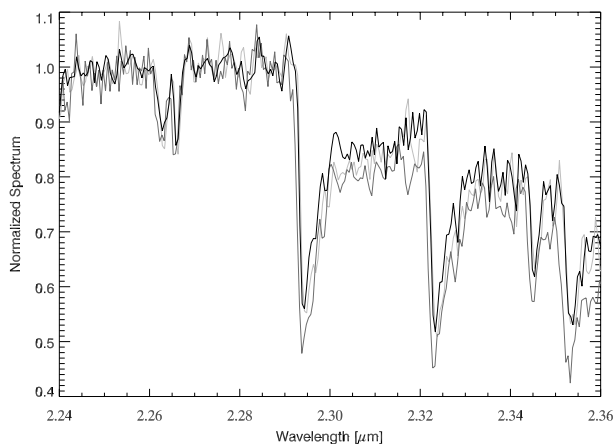


Fig. 6. SINFONI spectra. Only the three spectra with a resolution of ≈ 2000 are shown. *Dark gray:* MJD = 52 738, *black:* MJD = 55 383; *light gray:* MJD = 56 558.

erence magnitudes (GCIRS 16NE: $m_J = 14.01 \pm 0.08$, $m_H = 10.94 \pm 0.08$, $m_{Ks} = 9.01 \pm 0.05$ and $m_L = 7.56 \pm 0.09$ / GCIRS 16C: $m_J = 15.20 \pm 0.08$, $m_H = 11.96 \pm 0.08$, $m_{Ks} = 9.83 \pm 0.05$ and $m_L = 8.48 \pm 0.10$).

2.2.2. Archival Photometry

The star GCIRS 7 is the brightest individual source in the vicinity of Sgr A* in the near infrared. As such the star was targeted in many photometric surveys during the last decades. In an attempt to get a light-curve as long and complete as possible, we used all published J, H, Ks and L-band data that we were aware of. This includes data from Becklin & Neugebauer (1975), Depoy & Sharp (1991), Ott et al. (1999), Blum et al. (1996a) and Peeples et al. (2007). By comparing various stars (most notably GCIRS 16NE and 16C) in the published data sets (in particular Blum et al. 1996a), it turned out that the K-band data from Ott et al. (1999) seemed to be offset (brighter) on average by about 0.3 mag. This could be related to the choice of the magnitude reference star. To account for this difference, we added 0.3 magnitudes to the Ott et al. magnitudes. The combined light-curve is shown in Fig. 5.

2.3. SINFONI Spectroscopy

Our spectroscopic data (Fig. 6) were obtained with the adaptive optics assisted integral field spectrograph SINFONI (Eisenhauer et al. 2003; Bonnet et al. 2004). In total we used 4 observations obtained in April 2003 (MJD = 52 738), August 2004 (MJD = 53 237), July 2010 (MJD = 55 383) and September 2013 (MJD = 56 558) with pixel scales between 50×100 and 125×250 mas. The data output of SINFONI consists of cubes with two spatial axes and one spectral axis. Depending on the plate scale, an individual cube covers $3.2'' \times 3.2''$ or $8'' \times 8''$; the spectral resolving power was about 2 000 except for the 2004 run ($R \approx 4 000$). We used the data reduction SPRED (Schreiber et al. 2004; Abuter et al. 2006), including bad-pixel correction, flat-fielding and sky subtraction. The wavelength scale was calibrated with emission line gas lamps and fine-tuned on the atmospheric OH lines. Finally we removed the atmospheric absorption features by dividing the spectra through a telluric spectrum obtained in each respective night.

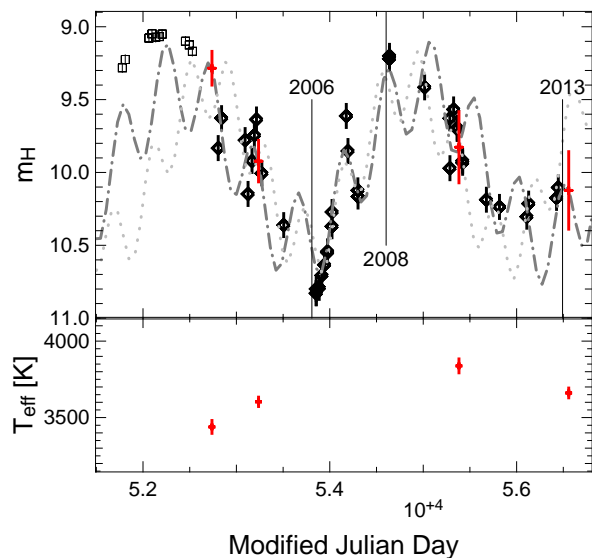


Fig. 7. *Top:* H-band light-curve after year 2000. *Bottom:* effective temperature measurements from SINFONI spectra. *Diamonds:* NACO data (fitted); *squares:* Peeples et al. (2007, for comparison). *Dash-dotted, dark grey curve:* best-fit two-period model. *Dotted, light grey curve:* second best-fit model. *Vertical lines:* dates of interferometric observations: March 2006 (Pott et al. 2008, K-band AMBER), May 2008 (K-band AMBER) and July 2013 (H-band PIONIER). *Crosses:* T_{eff} from SINFONI spectra and the corresponding magnitude estimated using the best fit model; the vertical line of each cross indicates the statistical uncertainty only (see text, Sect. 3.3).

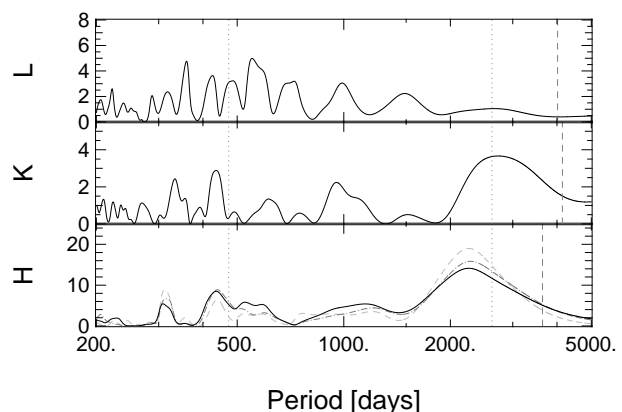


Fig. 8. Generalised Lomb–Scargle periodograms of the NACO light-curves (bottom to top: H, K and L-band). *Black curves:* data periodograms. *Light grey, dashed curve:* single-period model. *Dark grey, dash-dotted curve:* two-period model. *Vertical dotted lines:* best fit periods. *Vertical dashed lines:* NACO time coverage in each band. The periodograms are normalised so that the expected power for pure Gaussian noise is 1.

3. Results

The various physical parameters derived below, as well as a few complementary parameters from the literature, are summarised in Table 1.

3.1. Size

The H-band 2013 visibilities remain very high for spatial frequencies below $60 \text{ M}\lambda$ (i.e. $B_{\perp}/\lambda < 6 \times 10^7$ where B_{\perp} is the projected baseline length), except on the shortest baseline (U2–U3), for which the data have the lowest S/N. A decrease above $60 \text{ M}\lambda$

Table 1. Physical parameters

Parameter	Value	Uncertainty	Reference
<i>Direct measurements</i>			
$m_K(2013)$	7.31	± 0.07	Fig. 5
$m_H(2013)$	10.10	± 0.08	Fig. 5
$\langle m_K \rangle$	6.8	± 0.1	Fig. 5
$\langle m_H \rangle$	9.93	± 0.03	Table 2
P_{LT}	2850	d	Fig. 5
$\theta_{UD}(2013)$	1.076	± 0.093 mas	Sect. 3.1
P_0	470	± 10 d	Sect. 3.2
P_{LSP}	2620	± 140 d	Sect. 3.2
$\langle EW(CO) \rangle$	28	± 0.5	Fig. 10
<i>Indirect measurements</i>			
A_K	3.48	± 0.09	1
A_H/A_K	1.73	± 0.03	2
R_0	8.33	± 0.35 kpc	3
BC_K	2.84	± 0.15	4
$R_{UD}(2013)$	960	$\pm 92 R_\odot$	Sect. 3.1
$\langle T_{eff} \rangle$	3600	± 195 K	Table 3
$\langle M_K \rangle$	-11.3	± 0.16	Sect. 3.4
$\langle M_H \rangle$	-10.7	± 0.2	Sect. 3.4
$\langle M_{bol} \rangle$	-8.44	± 0.22	Sect. 3.4
$M_K(2013)$	-10.77	± 0.15	Sect. 3.4
$M_H(2013)$	-10.52	± 0.22	Sect. 3.4
$M_{bol}(2013)$	-7.93	± 0.21	Sect. 3.4
M	22.5	$\pm 2.5 M_\odot$	Sect. 3.5
Age	6.5–10	Myr	Sect. 3.5

Notes. $m_K(2013)$, $m_H(2013)$: K and H-band magnitudes measured in June and August 2013 respectively; $\langle m_K \rangle$, $\langle m_H \rangle$: baseline magnitudes; P_{LT} : long-term period; $\theta_{UD}(2013)$: best-fit uniform-disk angular diameter from the July 2013 PIONIER data; P_0 , P_{LSP} : fundamental and long secondary periods found from the H-band NACO data; $\langle EW(CO) \rangle$: average ^{12}CO equivalent width from the SINFONI data; A_K , A_H/A_K : K-band extinction correction and ratio of correction at H to K-band; R_0 : distance from the Sun to the GC; BC_K : bolometric correction for $T_{eff} = 3600$ K; $\langle T_{eff} \rangle$: average effective temperature; $R_{UD} = (2013)$: uniform-disk physical radius from the 2013 PIONIER data, taking limb-darkening into account would yield a 4% larger value; $M_{bol}(2013)$, $\langle M_{bol} \rangle$: 2013 and average bolometric magnitude; M : mass.

References. (1) Blum et al. (2003); (2) Nishiyama et al. (2009); (3) Gillessen et al. (2009); (4) Levesque et al. (2005).

($B_\perp > 100$ m at $\lambda = 1.68 \mu\text{m}$) is observed on the first night on the longest baseline (U2–U3), which also has a fairly low S/N, and on the second night on U1–U3. At any rate, $V^2 \gtrsim 0.7$ even at $73 M\lambda$. This points towards a barely resolved source, if at all.

Indeed, the best-fit uniform-disk diameter is only $\theta_{UD} = 1.076 \pm 0.093$ mas, corresponding to $R_{UD} \approx 960 \pm 92 R_\odot$ at 8.33 ± 0.35 kpc. To estimate a limb-darkened diameter, we have used the law of Claret (2000) and the coefficients for $T_{eff} = 3500$ K, $\log(g) = 0$, solar metallicity. The fitted value (4% larger than θ_{UD} , as expected) is the same within the statistical uncertainties: $\theta_{LD} = 1.116 \pm 0.098$ mas. In both cases, the reduced χ^2 is about 1.9 (the stated error bars are rescaled to account for the imperfect fits). The reduced χ^2 for $\theta_{UD} = 0$ (resp. 2) mas is ≈ 4 (resp. 9). Again, this shows that the source is only moderately resolved.

On the other hand, the K-band 2008 visibilities are of order $V^2 \approx 0.5$ for all baselines. This is a strong indication that up to 30% of the flux comes from a resolved environment, while $\gtrsim 70\%$ comes from a compact source. We have fitted a few models where the star is represented by a uniform disk and the en-

Table 2. Best-fit parameters for the two-period model

Parameter	Value	Uncertainty
P_0	470	± 10 d
a_0	0.32	± 0.05 mag
t_0	52360	± 40 d
P_{LSP}	2620	± 140 d
a_{LSP}	0.53	± 0.05 mag
t_{LSP}	53030	± 70 d
$\langle m_H \rangle$	9.93	± 0.03 mag

Notes. With t the modified Julian date:

$$m_H(t) = \langle m_H \rangle + a_0 \sin\left(2\pi \frac{t - t_0}{P_0}\right) + a_{LSP} \sin\left(2\pi \frac{t - t_{LSP}}{P_{LSP}}\right)$$

vironment is represented by a ring, a second uniform disk, or a uniform background. In all cases, the photospheric size is in the range $\theta_{UD} 1.5\text{--}2$ mas ($R_{UD} = 1340\text{--}1790 R_\odot$), the diameter of the circumstellar component is > 5 mas and the star accounts for 75–85% of the flux. These values should be considered with caution though, as the (u, v) coverage is not sufficient given the uncertainties to characterise both the stellar photosphere and the environment in details.

3.2. Light-Curve Periodicities

Figure 5 shows the photometric data described in Sect. 2.2.1 and 2.2.2. GCIRS 7 is clearly variable at J to L-band, as noted before in the literature. Our PIONIER H-band observations (modified Julian date $\text{MJD} \approx 56490$) as well as the 2006 AMBER observations presented in Pott et al. (2008, March 2006: $\text{MJD} \approx 53800$) occurred during a minimum of the star’s brightness. On the contrary, the AMBER K-band observations we present were acquired near a photometric maximum ($\text{MJD} = 54603$). The H-band magnitude measured on one NACO frame in June 2013 (resp. June 2008) was $m_H(2013) \approx 10.09$ (resp. $m_H(2008) \approx 9.21$).

For the first time, we are able to show that GCIRS 7 is semi-periodic at least at H-band with a long-term period of ≈ 2850 days (7.8 yr). The H-band light-curve samples very well the last two pseudo-periods, while Ott et al. (1999) K-band data cover the preceding period. The Becklin & Neugebauer (1975) data points are consistent with the extrapolated sine curves, while the Depoy & Sharp (1991) points (observed in 1989 and 1990) are too bright at all wavelengths.

The single periodicity sine-curve model is a fair representation of the light-curve variations, but departures from this model are significant. In particular, shorter term variations are seen in the NACO data (Fig. 7). Furthermore, RSGs are known to often exhibit semi-periodic variations. Many stars show a short period (P_0 , on the order of few 100 days) which is well explained by the fundamental mode or first overtone of radial pulsation. Other stars show in addition or instead a longer period ($P_{LSP} > 1000$ d) referred to as the long secondary period (LSP), which is less well explained (see Kiss et al. 2006, and references therein).

Our time sampling is good only for the NACO era, and there it extends only for a little more than one period. We have constructed the generalised Lomb–Scargle periodograms (Fig. 8, Lomb 1976; Scargle 1982; Zechmeister & Kürster 2009) for the H, K and L-band NACO data which contain data for respectively 37, 20, and 13 distinct dates over 3641, 4142 and 4015 days and attempted simple model fitting of one or two sine curves.

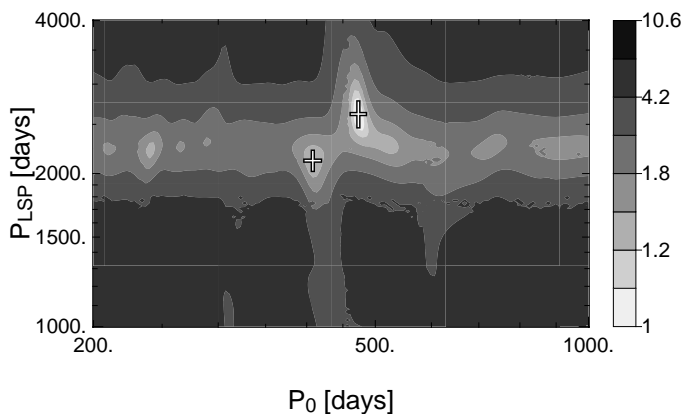


Fig. 9. χ^2 map for the two-period H-band model, normalised to its minimum of 4.68. The best-fit period pairs are marked by uncertainty crosses.

The χ^2 map of the two-period model (Fig. 9) shows that there are only two pairs of periods able to reproduce the NACO data decently, fairly close to each other: $(P_0, P_{LSP}) = (410 \pm 10 \text{ d}, 2120 \pm 88 \text{ d})$ and $(470 \pm 10, 2620 \pm 140)$. They cannot be distinguished using a χ^2 argument alone. However, the second pair is closer to the longer term period seen on Fig. 5 and fits the Peeples et al. (2007) data points better (Fig. 7). This is therefore the solution we consider as best. The 7 best-fit parameters are listed in Table 2. The amplitudes associated with the two periods are of the same order: respectively 0.6 ± 0.1 and 1.1 ± 0.1 mag peak-to-peak for the short and long periods. Although still not perfect (reduced $\chi^2 = 4.7$), this two-period model reproduces the data (Fig. 7) and their power-spectrum (Fig. 8) much better than the single-period model (reduced $\chi^2 = 10.4$).

The K-band light-curve from the NACO era appears almost constant at $m_K = 7$, except the first point around $m_K = 6.5$. The most prominent feature of the K-band periodogram is a broad peak, around 2800 d, compatible with both the long-term period (2850 d) and the short-term H-band P_{LSP} (2620 d). We tried fitting one or two periods on the K-band data as well as fitting only the amplitudes for two sine curves at the periods and phases determined from the H-band data. The reduced χ^2 for the three different fits remains approximately the same. In conclusion, the K-band data are in favour of $P_{LSP} \approx 2800$ d, compatible with P_0 obtained from the H-band data, but do not bring further constraints.

Finally, the L-band periodogram is dominated by a band of lines around 500 d, which could be the signature of P_0 seen in the H-band data. The data sampling does not allow asserting this firmly, though.

3.3. Effective Temperature

Cool stars with temperatures between 3000–5000 K show prominent CO absorption features between 2.29 and 2.40 μm . The CO absorption strength varies sensitively with temperature, which makes the so-called CO band heads excellent tracers for the stellar temperature. Numerous definitions of the CO equivalent width have been proposed in the literature (e.g. Kleinmann & Hall 1986; Frogel et al. 2001). Previous studies of the cool stellar population in the GC such as Blum et al. (2003), Maness et al. (2007) and Pfuhl et al. (2011) determined accurate $^{12}\text{CO}(2,0)-T_{\text{eff}}$ calibrations, yet only for giant stars. The CO strength however not only depends on the effective temperature but also on surface gravity. Therefore to get reliable temperature

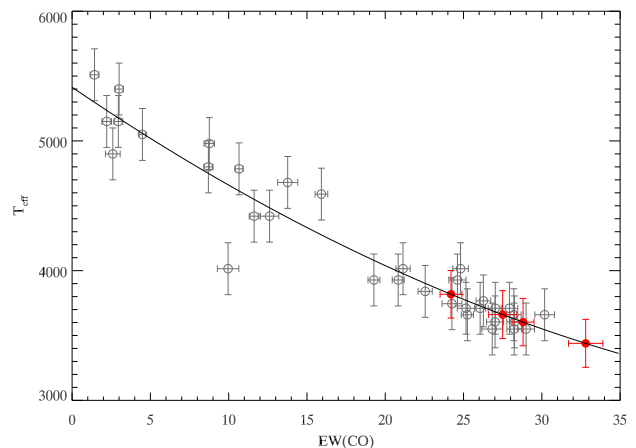


Fig. 10. CO- T_{eff} calibration for RSGs with spectral types between G0 and M4. *Open circles*: stars from the IRTF library. The temperature uncertainty of the individual stars is 200 K (Allen & Cox 2000). *Curve*: best-fit empirical relation. *Filled circles*: EW(CO) measurements on GCIRS 7 and derived T_{eff} .

estimates for the RSG GCIRS 7, it is necessary to determine an adequate $^{12}\text{CO}(2,0)-T_{\text{eff}}$ calibration for RSGs.

In order to setup such a calibration we used 34 published RSG spectra ($R \approx 2000$) from the IRTF library (Rayner et al. 2009). The template spectra comprise stars with luminosity classes between Ia to Ib and spectral types between G0 and M4. We measured the CO strength according to the definition of Frogel et al. (2001) since their index proved to be insensitive to biases (Pfuhl et al. 2011). The effective temperature of the library stars was derived based on their spectral type. For spectral types between G0 and K0 we used temperatures from (Allen & Cox 2000, p. 152). In case of later spectral types K1 to M5, we used the revised calibration from Levesque et al. (2005). The result is shown Fig. 10. As expected, the CO strength clearly correlates with the stellar temperature. We used a 2nd-order polynomial fit get an empirical relation between EW(CO) and effective temperature. The best-fit relation is:

$$T_{\text{eff}} = 0.669 \cdot \text{CO}^2 - 82.139 \cdot \text{CO} + 5414 \text{ [K]} \quad (1)$$

The intrinsic scatter of the template stars with respect to the best-fit temperature is 180 K. This is roughly consistent with the stated temperature uncertainty of the spectral types of ~ 200 K (Allen & Cox 2000, p. 153). All available temperature measurements are summarised in Table 3. Although the measurements used various techniques, they all agree very well. In the following, we use the mean of the measurements $\langle T_{\text{eff}} \rangle = 3600 \pm 195$ K as an estimate of the average temperature of the star. The uncertainty is the mean of the individual uncertainties and is dominated by systematic errors. The root-mean-square scatter between the individual measurements is only 116 K.

Even though the systematic errors are too large to derive a consistent temperature curve, EW(CO) does change measurably between SINFONI runs (Fig. 10), and the colours also vary quite significantly. We investigate the temperature variations by considering only the statistical uncertainties in the four SINFONI T_{eff} estimates, assuming that the systematic effects affect those four points in the same fashion. We have also estimated the H-band magnitude of the star at the corresponding dates using our best fit model (Table 2). We used uncertainties on the fit param-

Table 3. Effective temperature of GCIRS 7

Date (MJD)	T_{eff} [K] ²	Reference
56 558	$3\,661 \pm 185$...
55 383	$3\,818 \pm 183$...
53 237	$3\,603 \pm 183$...
52 738	$3\,439 \pm 185$...
52 426	$3\,650 \pm 150$	1
51 332	$3\,600 \pm 200$	2
50 648	$3\,430 \pm 240$	3
49 122	$3\,600 \pm 230$	4
Average	$3\,600 \pm 195$...

Notes. All uncertainties include systematic errors. For the SINFONI data set, 180 K have been added in quadrature to the statistical uncertainties to this effect.

References. (1) Cunha et al. (2007); (2) Davies et al. (2009); (3) Blum et al. (2003); (4) Carr et al. (2000).

Table 4. Variations of T_{eff} , M_{H} and R_{LD} from the SINFONI spectra and NACO H-band photometry

MJD	T_{eff} [K]	M_{H}	R_{LD} [R_{\odot}]
56 558	$3\,661 \pm 32$	10.1 ± 0.3	950 ± 120
55 383	$3\,838 \pm 45$	9.8 ± 0.2	1030 ± 120
53 237	$3\,603 \pm 31$	9.9 ± 0.1	1068 ± 71
52 738	$3\,439 \pm 42$	9.3 ± 0.1	1524 ± 85

Notes. In this table, only statistical uncertainties are considered. For instance, when propagating also systematic sources of error, the uncertainty on R_{LD} reaches $200 R_{\odot}$ for 2003.

ters to derive uncertainties on these magnitudes. Those temperatures, magnitudes and the corresponding uncertainties are shown Fig. 7.

To assess the significance of the variation in T_{eff} between SINFONI runs, we first take the average of these four values: $\langle T_{\text{eff}} \rangle_{\text{SINFONI}} = 3\,629 \pm 18$ K. The departure from this value for each date is respectively -190 ± 46 , -26 ± 36 , 209 ± 49 and 32 ± 36 K. This is on average a 2.5σ departure.

3.4. Absolute Magnitude and Bolometric Luminosity

The intrinsic K and H-band luminosity of GCIRS 7 can be derived from the average observed $\langle m_{\text{K}} \rangle = 6.8 \pm 0.1$ and $\langle m_{\text{H}} \rangle = 9.93 \pm 0.03$, the measured K-band extinction $A_{\text{K}} = 3.48 \pm 0.09$ (Blum et al. 2003) and $A_{\text{H}}/A_{\text{K}} = 1.73 \pm 0.03$, (Nishiyama et al. 2009; Fritz 2013) and the distance modulus $d = 14.6 \pm 0.09$ (assuming $R_0 = 8.33 \pm 0.35$ kpc, Gillessen et al. 2009). The absolute, dereddened K and H-band magnitudes are therefore $\langle M_{\text{K}} \rangle = -11.3 \pm 0.16$ and $\langle M_{\text{H}} \rangle = -10.7 \pm 0.2$. The bolometric K-band correction for a star with $T_{\text{eff}} = 3\,600 \pm 195$ K is $\text{BC}_{\text{K}} = 2.84 \pm 0.15$ (Levesque et al. 2005). Thus the (average) absolute bolometric magnitude of GCIRS 7 is $\langle M_{\text{bol}} \rangle = -8.44 \pm 0.22$, corresponding to a luminosity of $\langle L \rangle = 1.86 \pm 0.4 \times 10^5 L_{\odot}$. The position of GCIRS 7 in the Hertzsprung–Russell (HR) diagram can be seen in Fig. 11.

Likewise, the 2013 values of the K and H-band and bolometric absolute magnitudes are $M_{\text{K}}(2013) = -10.77 \pm 0.15$, $M_{\text{H}}(2013) = -10.52 \pm 0.22$ and $M_{\text{bol}}(2013) = -7.93 \pm 0.22$ respectively.

To estimate the bolometric magnitude of the star at the time of the SINFONI observations, we lack a well-established H-band bolometric correction law. However, using T_{eff} , m_{H} , and the rela-

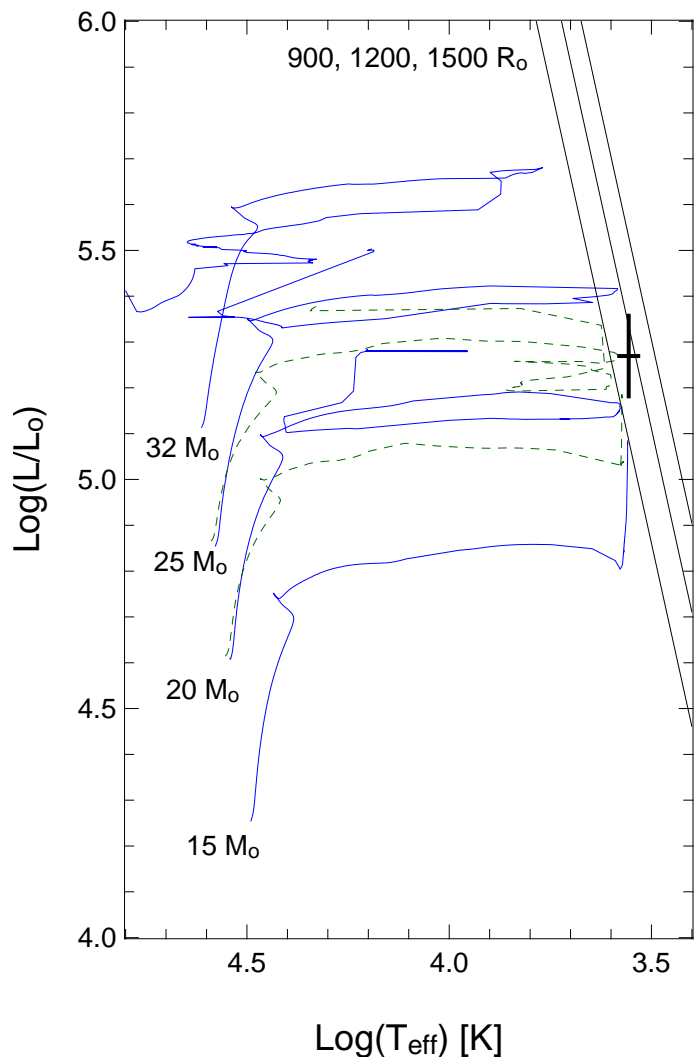


Fig. 11. Position of GCIRS 7 in the H-R diagram (cross) compared with evolutionary tracks of stars with initial masses between $M_{\text{ini}} = 15 - 32 M_{\odot}$ with rotation (blue solid) and for $M_{\text{ini}} = 20 - 25 M_{\odot}$ without rotation (dashed green) from Ekström et al. (2012). The solid black lines denote the theoretical luminosities of stars with radii of $R = 900, 1100$ and $1300 R_{\odot}$ as function of effective temperature.

tions in Kervella et al. (2004), we can derive the radius of the star for these four epochs. From these radii and the temperatures, we can directly get the bolometric magnitude at each SINFONI observation. In this estimation, we are only interested in the statistical uncertainties and therefore do not consider the uncertainties on A_{K} , $A_{\text{H}}/A_{\text{K}}$ and R_0 . The values are listed in Table 4.

3.5. Age and initial mass

In order to estimate the initial mass and the age of GCIRS 7, we rely on the recent evolutionary tracks from Ekström et al. (2012, Fig. 11). Their tracks include stellar rotation and assume a solar metallicity. This seems to be a reasonable choice since GCIRS 7 is known to have a metallicity close to solar (Carr et al. 2000; Cunha et al. 2007). GCIRS 7 falls between the evolutionary tracks of $M_{\text{ini}} = 20 M_{\odot}$ and $M_{\text{ini}} = 25 M_{\odot}$ stars with and without rotation. Stars with initial masses of $M_{\text{ini}} = 20 M_{\odot}$ reach the RSG phase after about 8 Myr without rotation and 10 Myr with rotation and last there for about 0.2 Myr. Stars with initial masses of $25 M_{\odot}$ reach the RSG phase after about 6.5 Myr

without and after 8 Myr with rotation and remain there for a few ten thousand years. Stars with initial masses of $15 M_{\odot}$ (RSG age 14–15 Myr) do not reach the observed luminosity. Unfortunately evolutionary tracks with a finer mass sampling are available only through an interpolation tool³. GCIRS 7 lies on the far right end of the tracks, and the interpolation seems to cut some of this temperature extremum. The authors of the interpolation tools note that it can not be relied upon for unstable phases. However the available tracks (as well as the interpolated tracks) are roughly equally spaced in luminosity. Based on that we estimate that GCIRS 7 originates from a star with initial mass of $22.5 \pm 2.5 M_{\odot}$ (in good agreement with Cunha et al. 2007, $22 M_{\odot}$). Depending on the initial rotation of the star, the age of GCIRS 7 is in the range 6.5–10 Myr.

4. Discussion

4.1. On the size of GCIRS 7 and its environment

The effective temperature and radius of 74 Galactic RSGs has been determined by van Belle et al. (2009). From their equation (1), we can estimate $(V - K)_0 = 4.5 \pm 0.3$ for GCIRS 7. This part of their Fig. 5 ($(V - K)_0 > 3.5$, $R > 500 R_{\odot}$) is mostly occupied by stars from Levesque et al. (2005), with which GCIRS 7 is quite consistent.

Using $T_{\text{eff}} = 3600$ K, $m_{\text{H}}(2013) = 10.10$, $A_K = 3.48$ and $A_H/A_K = 1.73$ (Table 1), we compute a limb-darkened diameter of 1.10 mas using the relations given in Kervella et al. (2004). The K-band relation with $m_K(2013) = 7.3$ yields a very similar value. This is well within 1σ of our 2013 measurement. The angular diameter we fitted on the 2008 K-band AMBER data (1.5–2 mas) is affected by degeneracy with the circumstellar environment. However, it is consistent with the photometry: the H-band relation in Kervella et al. 2004 yields $\theta_{\text{LD}} = 1.68$, $R_{\text{LD}} = 1500 R_{\odot}$ for $m_{\text{H}}(2008) = 9.21$, still assuming $T_{\text{eff}} = 3600$ K. In addition, this diameter is also consistent with the value we determine spectro-photometrically for the 2003 epoch, at which the star was approximately as bright as in 2008 (Table 4, Fig. 7).

The question which arises is whether this apparent change in radius is real. Indeed, no radius pulsation has been detected so far on similar RSGs. A change from $\approx 1000 R_{\odot}$ to $1500 R_{\odot}$ translates to $\Delta R/R \approx 40\%$, which is somewhat larger than the maximum amplitude observed in cepheids (Tsvetkov 1988). In addition, $R \approx 1500 R_{\odot}$ is the size of the largest known RSGs (Levesque et al. 2005; Arroyo-Torres et al. 2013). Our interferometric measurements hint at a change of diameter. This change is confirmed by our analysis of the available spectroscopy and photometry. However, the systematic uncertainty of T_{eff} translates into a large ($\approx 200 R_{\odot}$) systematic uncertainty on the radius. In addition, the spectro-photometric estimates assume that the H-band local extinction was constant throughout the 10 years. Furthermore, the largest estimate ($R_{\text{LD}}(2003) = 1500 \pm 200 R_{\odot}$, including systematic errors) is based on an extrapolation of the NACO light-curve. In conclusion, the unique best direct measurement for the size of GCIRS 7 is our PIONIER 2013 H-band measurement, which is not subject to degeneracy with the circumstellar environment, the star is probably truly variable in size, and θ_{UD} is unlikely to reach values in excess of 1.7 mas ($R \approx 1500 R_{\odot}$).

This confirms the interpretation in Pott et al. (2008), where the loss of visibility was eventually attributed to a circumstel-

lar contribution. However, the visibility measured in 2006 at K-band in Pott et al. (2008) was actually quite high compared to our 2008 measurement ($V^2 \approx 0.8$ at $\approx 20 M\lambda$). Since the star was very faint at that time, one would naively expect the circumstellar emission to dominate and therefore the visibility to be quite low. This was not the case. This means that not only the star, but also its environment has varied between 2006 and 2008. The 2006 measurement can be understood with either (or both) of the following hypotheses:

- the circumstellar emission was fainter in 2006 than in 2008, so that the ratio of one over the other has not changed much;
- the circumstellar emission was more compact when the star itself was smaller and fainter, such that the visibility of the extended component was larger in 2006 than in 2008.

A circumstellar contribution could also explain why the K-band (and L-band) magnitude has not varied much in the last decade: photospheric variations at longer wavelengths are perhaps diluted in a significant, steady circumstellar emission. This does not explain, however, why the star appears to have been fainter at K-band in recent years compared to what it was at the end of the XXth century. Obscuration by newly formed circumstellar material is not a very tempting explanation, as it would have impacted H-band photometry even stronger than K-band photometry. In addition, this extended component would need to be emission rather than scattering, since scattering is more efficient at shorter wavelengths. Black-body emission from dust could have a significant contribution at K-band while remaining basically undetectable from our H-band PIONIER data. Finally, A_K is larger by ≈ 1 mag in the direction of GCIRS 7 compared to the rest of the central parsec (Schödel et al. 2010), which points towards a fairly thick circumstellar environment.

As mentioned in the introduction, ISM features North of GCIRS 7 have been interpreted as the outer layers of the star's atmosphere being blown away by the central cluster wind in a cometary tail (Serabyn et al. 1991; Yusef-Zadeh & Morris 1991). Another evidence of this cluster wind is provided by the very clear, large-scale bow-shock South-East of GCIRS 3 (Viehmann et al. 2005). The fact that our size measurement is quite consistent with the bolometric magnitude and effective temperature of the star tends to show that the interaction with the cluster wind does not affect the photospheric appearance of the star nor, presumably, its mass-loss rate. Further investigations, however, should be able to measure the actual distribution of circumstellar material around the star.

4.2. On the variability of GCIRS 7

The short, primary period of RSGs follows a fairly tight period-luminosity (P-L) relation (Yang & Jiang 2012, and references therein). Figure 12 presents GCIRS 7 ($M_K = -11.3 \pm 0.16$, $M_H = -10.7 \pm 0.2$, $P_0 = 470 \pm 10$ d, see Table 1) on the P-L relationship for RSGs in the SMC and LMC. Given the uncertainty on the absolute magnitudes of GCIRS 7 and the intrinsic scatter around the best-fit relation, the agreement with the P-L relation is quite good, especially at H-band. The K-band magnitude of the star appears to be ≈ 0.1 mag too bright, which could be due to the circumstellar contribution discussed Sect. 4.1.

In contrast to the short, primary period of RSGs, there is as of now no P-L relation established for the LSP. However, Kiss et al. (2006) have noticed a relation between the LSP, mass and radius of RSGs. They considered $W = P(M/M_{\odot})(R/R_{\odot})^{-2}$, which “is the natural form of the pulsation constant if the oscillations are confined to the upper layers of the envelope (Gough et al. 1965)”.

³ <http://obswww.unige.ch/Recherche/evoldb/index/Interpolation/>

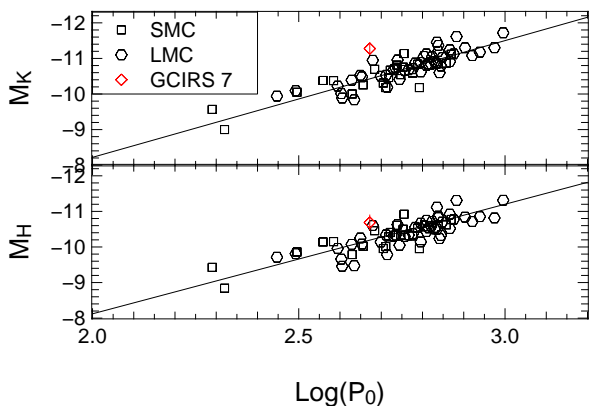


Fig. 12. Period-Luminosity relation for RSGs. *Diamond with vertical error bar:* GCIRS 7. *Squares and circles:* SMC and LMC stars used in Yang & Jiang (2012). *Line:* best-fit law for the LMC+SMC (Yang & Jiang 2012, Table 5).

They computed the average of W for 14 RSGs with $P > 1000$ d and found $\langle W \rangle = 0.082 \pm 0.03$. Taking $P = 2620\text{--}2850$ d, $\langle R \rangle = 1000 R_{\odot}$ and $M = 22.5 M_{\odot}$ (Table 1, Sect. 4.1), we find for GCIRS 7 $W = 0.059\text{--}0.064$, within 1σ of the above mentioned average.

4.3. GCIRS 7 as an interferometric calibrator for GRAVITY

GCIRS 7 is the only star in the central parsec bright enough to be used as fringe-tracker reference with GRAVITY operating on the VLTI auxiliary telescopes (ATs). Furthermore, this star being bright and close from the central black-hole candidate Sgr A*, it will be tempting to use it as a visibility calibrator whenever observing an object in the central parsec with GRAVITY, be it with the UTs or with the ATs.

However, GRAVITY will operate in the K-band. The K-band visibilities of GCIRS 7 are affected by a significant, variable circumstellar contribution (Sect. 4.1). It will therefore be difficult to use this star as a visibility calibrator. Nevertheless, assuming the circumstellar geometry is simple enough (pending further investigations), one could perhaps use the star as a local calibration proxy. At any rate, the star must be considered interferometrically variable on the time scale of about one month, a fraction of the ≈ 470 d short period that we measured.

In addition, the size and nature of GCIRS 7 imply that convection cells may form in its atmosphere and impact the appearance of the photosphere (see e.g. Haubois et al. 2009; Freytag & Höfner 2008). Chiavassa et al. (2011) have shown that the photometric wobbling for a Betelgeuse-like star is of order 0.1 AU, corresponding to $\approx 10 \mu\text{as}$ at the distance of the Galactic Centre. This is of the same order as the expected astrometric accuracy of GRAVITY itself. This will limit the astrometric precision of studies of the nuclear star cluster using GCIRS 7 as astrometric reference. This limitation may be alleviated by systematically calibrating the astrometric zero point by observing one or several smaller or more stable stars.

4.4. On the age of GCIRS 7 and the recent star burst

We list various physical parameters in Table 1, which are all consistent with each other. This gives good confidence in the age we derive for GCIRS 7: 6.5 to 10 Myr, depending on rotation.

RSGs are in a rare state. The ratio of red to blue supergiants is approximately 0.4–0.5% (e.g. Pfuhl et al. 2011), so that there

must be approximately 200 blue supergiants in the Galactic Centre with the same age as GCIRS 7. There is a unique, well known population of > 100 hot, massive stars in the central parsec, and the age we derive for GCIRS 7 is consistent the age estimated by several authors for this population (2–7 Myr, Genzel et al. 2003; 6 ± 2 Myr Paumard et al. 2006; Bartko et al. 2009). On the other hand, Lu et al. (2013) derived a 95% confidence interval for a cluster age of 2.5 to 5.8 Myr. This claim is not compatible with the age we derive for GCIRS 7.

Lu et al. (2013) relied essentially on the ratio of Wolf-Rayet (WR) to OB stars. This method has been recognised to be strongly dependent on the prediction of evolutionary tracks (Schaerer & Vacca 1998). The evolution of a star beyond the main sequence, especially in the WR phase, is very sensitive to numerical and physical prescriptions such as overshooting and mass loss rate. For an illustration, see e.g. Martins & Palacios (2013). In addition, the definition of a WR star does not rely on the same criteria in evolutionary models and in spectroscopic surveys. Finally, it is crucial to have complete sample to correctly evaluate the observed ratio of WR to OB stars.

This is why in Paumard et al. (2006) we did not rely only on this indicator. In addition, we looked for the turn-off in the HR diagram (Paumard et al. 2006, Fig. 12), i.e. the position in the HR diagram of the most massive stars in the main sequence. The age of GCIRS 7 is a now third independent age indicator. Taken together, these indicators point towards a cluster age in the range 6–8 Myr. This age is actually permitted by the error bars of Fig. 3, right panel, of Lu et al. (2013), especially if one allows for a slightly flatter initial mass function than their preferred slope.

The simultaneous presence of both RSG and WR stars in a massive cluster presumably formed in a single burst of star formation is rare. For that to happen, the cluster must be young enough for the most massive stars to still be present (in the WR phase). At the same time, it must be old enough so that stars in the mass range 10–25 M_{\odot} have evolved to the RSG phase. The fact that we are able to explain the presence of OB, WR stars and the RSG GCIRS 7 using a single isochrone is a very strong indication that the central cluster is in this peculiar age range where all types of stars are present.

5. Conclusions

We have obtained interferometric fringes on GCIRS 7 with PIONIER on the six UT baselines of the VLTI at H-band. We have been able to measure the photospheric size of the star: $\theta_{\text{UD}}(2013) \approx 1.076 \pm 0.093$ mas translating to $R_{\text{UD}}(2013) \approx 960 \pm 92 R_{\odot}$ at $R_0 = 8.33 \pm 0.35$ kpc. K-band AMBER observations obtained in 2008 show a significant ($\approx 20\%$) circumstellar excess, and hint at photospheric and circumstellar variations. Photospheric temperature and size variations are confirmed by spectroscopy and photometry.

In addition, we have reanalysed near infrared light-curves of the star and found a prominent, long period of 2620–2850 days and a shorter period of 470 ± 10 days. The global peak-to-peak variation has been ≈ 2 mag at H-band and ≈ 1.6 mag at K-band during the last 40 yr. The size we measure is quite consistent with the luminosity ($\langle M_{\text{bol}} \rangle = -8.44 \pm 0.22$) and effective temperature ($T_{\text{eff}} = 3600 \pm 195$ K) of the star, and the short and long periods are in good agreement with the fundamental and long secondary period respectively for a RSG that size and that mass ($22.5 \pm 2.5 M_{\odot}$, Sect. 3.5). The physical parameters we derive are listed in Table 1.

Future observations of the Galactic Centre nuclear star cluster may be performed with GRAVITY using GCIRS 7 as a

fringe-tracker reference. Given the variable nature of this star and its environment, it may not be a stable phase reference at the expected accuracy of GRAVITY ($10 \mu\text{as}$) for durations of more than a few weeks. Therefore, it may be useful to calibrate the astrometric zero-point on smaller or more stable stars regularly when using GCIRS 7 as a phase reference. Likewise, its usability as a (secondary) K-band visibility calibrator depends on whether the environment morphology is simple enough, pending further investigations.

Finally, the age we derive (6.5–10 Myr) is a confirmation of the cluster age (6 ± 2 Myr) we determined (Paumard et al. 2006; Bartko et al. 2009) and contradicts recent claims for a younger cluster (2.5–5.8 Myr, Lu et al. 2013).

Acknowledgements. We thank Myriam Benisty for help with the AMBER data reduction. This research has made use of Jean-Marie Mariotti Center products: the AMBER data reduction package⁴ and the LITpro⁵ service (Tallon-Bosc et al. 2008) co-developed by CRAL, LAOG and FIZEAU, as well as of NASA's Astrophysics Data System. We acknowledge financial support from the "Programme National de Physique Stellaire" (PNPS) of CNRS/INSU, France.

References

- Abuter, R., Schreiber, J., Eisenhauer, F., et al. 2006, *New A Rev.*, 50, 398
- Allen, C. & Cox, A. 2000, *Allen's astrophysical quantities* (AIP Press)
- Arroyo-Torres, B., Wittkowski, M., Marcaide, J. M., & Hauschildt, P. H. 2013, *A&A*, 554, A76
- Bartko, H., Martins, F., Fritz, T. K., et al. 2009, *ApJ*, 697, 1741
- Becklin, E. E. & Neugebauer, G. 1968, *ApJ*, 151, 145
- Becklin, E. E. & Neugebauer, G. 1975, *ApJ*, 200, L71
- Blum, R. D., Ramírez, S. V., Sellgren, K., & Olsen, K. 2003, *ApJ*, 597, 323
- Blum, R. D., Sellgren, K., & Depoy, D. L. 1996a, *ApJ*, 470, 864
- Blum, R. D., Sellgren, K., & Depoy, D. L. 1996b, *AJ*, 112, 1988
- Bonnet, H., Abuter, R., Baker, A., et al. 2004, *The Messenger*, 117, 17
- Carr, J. S., Sellgren, K., & Balachandran, S. C. 2000, *ApJ*, 530, 307
- Chelli, A., Utrera, O. H., & Duvert, G. 2009, *A&A*, 502, 705
- Chiavassa, A., Pasquato, E., Jorissen, A., et al. 2011, *A&A*, 528, A120
- Claret, A. 2000, *A&A*, 363, 1081
- Cunha, K., Sellgren, K., Smith, V. V., et al. 2007, *ApJ*, 669, 1011
- Davies, B., Origlia, L., Kudritzki, R.-P., et al. 2009, *ApJ*, 694, 46
- Depoy, D. L. & Sharp, N. A. 1991, *AJ*, 101, 1324
- Eisenhauer, F., Abuter, R., Bickert, K., et al. 2003, in *Society of Photo-Optical Instrumentation Engineers (SPIE) Conference Series*, Vol. 4841, Society of Photo-Optical Instrumentation Engineers (SPIE) Conference Series, ed. M. Iye & A. F. M. Moorwood, 1548–1561
- Eisenhauer, F., Perrin, G., Rabien, S., et al. 2008, in *The Power of Optical/IR Interferometry: Recent Scientific Results and 2nd Generation*, ed. A. Richichi, F. Delplancke, F. Paresce, & A. Chelli, 431
- Ekström, S., Georgy, C., Eggenberger, P., et al. 2012, *A&A*, 537, A146
- Freytag, B. & Höfner, S. 2008, *A&A*, 483, 571
- Fritz, T. 2013, PhD thesis, Ludwig-Maximilians-Universität, Munich
- Frogel, J. A., Stephens, A., Ramírez, S., & DePoy, D. L. 2001, *AJ*, 122, 1896
- Genzel, R., Eisenhauer, F., & Gillessen, S. 2010, *Reviews of Modern Physics*, 82, 3121
- Genzel, R., Schödel, R., Ott, T., et al. 2003, *ApJ*, 594, 812
- Gillessen, S., Eisenhauer, F., Trippe, S., et al. 2009, *ApJ*, 692, 1075
- Gough, D. O., Ostriker, J. P., & Stobie, R. S. 1965, *ApJ*, 142, 1649
- Haubois, X., Perrin, G., Lacour, S., et al. 2009, *A&A*, 508, 923
- Kervella, P., Thévenin, F., Di Folco, E., & Ségransan, D. 2004, *A&A*, 426, 297
- Kiss, L. L., Szabó, G. M., & Bedding, T. R. 2006, *MNRAS*, 372, 1721
- Kleinmann, S. G. & Hall, D. N. B. 1986, *ApJS*, 62, 501
- Krabbe, A., Genzel, R., Eckart, A., et al. 1995, *ApJ*, 447, L95
- Le Bouquin, J.-B., Berger, J.-P., Lazareff, B., et al. 2011, *A&A*, 535, A67
- Lenzen, R., Hartung, M., Brandner, W., et al. 2003, in *Society of Photo-Optical Instrumentation Engineers (SPIE) Conference Series*, Vol. 4841, Society of Photo-Optical Instrumentation Engineers (SPIE) Conference Series, ed. M. Iye & A. F. M. Moorwood, 944–952
- Levesque, E. M., Massey, P., Olsen, K. A. G., et al. 2005, *ApJ*, 628, 973
- Lomb, N. R. 1976, *Ap&SS*, 39, 447
- Lu, J. R., Do, T., Ghez, A. M., et al. 2013, *ApJ*, 764, 155
- Maness, H., Martins, F., Trippe, S., et al. 2007, *ApJ*, 669, 1024
- Martins, F. & Palacios, A. 2013, *A&A*, 560, A16
- Nishiyama, S., Tamura, M., Hatano, H., et al. 2009, *ApJ*, 696, 1407
- Ott, T., Eckart, A., & Genzel, R. 1999, *ApJ*, 523, 248
- Pauls, T. A., Young, J. S., Cotton, W. D., & Monnier, J. D. 2005, *PASP*, 117, 1255
- Paumard, T., Genzel, R., Martins, F., et al. 2006, *ApJ*, 643, 1011
- Peeples, M. S., Stanek, K. Z., & Depoy, D. L. 2007, *Acta Astron.*, 57, 173
- Pfuhl, O., Fritz, T. K., Zilka, M., et al. 2011, *ApJ*, 741, 108
- Pott, J.-U., Eckart, A., Glindemann, A., et al. 2008, *A&A*, 487, 413
- Rayner, J. T., Cushing, M. C., & Vacca, W. D. 2009, *ApJS*, 185, 289
- Rousset, G., Lacombe, F., Puget, P., et al. 2003, in *Society of Photo-Optical Instrumentation Engineers (SPIE) Conference Series*, Vol. 4839, Society of Photo-Optical Instrumentation Engineers (SPIE) Conference Series, ed. P. L. Wizinowich & D. Bonaccini, 140–149
- Scargle, J. D. 1982, *ApJ*, 263, 835
- Schaerer, D. & Vacca, W. D. 1998, *ApJ*, 497, 618
- Schödel, R., Najarro, F., Muzic, K., & Eckart, A. 2010, *A&A*, 511, A18
- Schreiber, J., Thatte, N., Eisenhauer, F., et al. 2004, in *Astronomical Society of the Pacific Conference Series*, Vol. 314, *Astronomical Data Analysis Software and Systems (ADASS) XIII*, ed. F. Ochsenbein, M. G. Allen, & D. Egret, 380–+
- Serabyn, E., Lacy, J. H., & Achtermann, J. M. 1991, *ApJ*, 378, 557
- Tallon-Bosc, I., Tallon, M., Thiébaud, E., et al. 2008, in *Society of Photo-Optical Instrumentation Engineers (SPIE) Conference Series*, Vol. 7013, Society of Photo-Optical Instrumentation Engineers (SPIE) Conference Series
- Tatulli, E., Millour, F., Chelli, A., et al. 2007, *A&A*, 464, 29
- Tsvetkov, T. G. 1988, *Ap&SS*, 150, 223
- van Belle, G. T., Creech-Eakman, M. J., & Hart, A. 2009, *MNRAS*, 394, 1925
- Viehmann, T., Eckart, A., Schödel, R., et al. 2005, *A&A*, 433, 117
- Yang, M. & Jiang, B. W. 2012, *ApJ*, 754, 35
- Yusef-Zadeh, F. & Morris, M. 1991, *ApJ*, 371, L59
- Zechmeister, M. & Kürster, M. 2009, *A&A*, 496, 577

⁴ Available at <http://www.jmmc.fr/amberdrs>

⁵ LITpro software available at <http://www.jmmc.fr/litpro>